ADVANCED MATERIALS INTERFACES
www.advmatinterfaces.de

Diamond Surfaces with Clickable Antifouling Polymer Coating for Microarray-Based Biosensing

Ravi Kumar, Bingquan Yang, Jan Barton, Miroslava Stejfova, Andreas Schäfer, Meike König, Peter Knittel, Petr Cigler, and Michael Hirtz**

Diamond enables the construction of various (bio)sensors, including those with quantum-based detection. However, bare diamond interfaces are susceptible to unspecific adhesion of proteins and other macromolecules from biological media or complex samples. This impairs selectivity in biosensing, leads to low signal-to-noise ratio in fluorescence-based applications, and introduces the need for blocking steps in incubation protocols. Here, a stable, protein-repellent, and clickable reactive polymer coating is introduced, abolishing unspecific protein adhesion while concurrently enabling covalent immobilization of functional compounds as recognition elements. The polymer coating has two segments, an antifouling poly(*N*-(2-hydroxypropyl) methacrylamide) and an alkyne-terminated poly(propargyl methacrylamide) providing the click functionality. The antifouling properties and click-reactivity of the polymers are demonstrated by selective protein binding assays on micropatterns written by microchannel cantilever spotting (µCS). The assays demonstrated the successful functionalization of both diamond and glass surfaces and the excellent antifouling properties of the polymer coating. The coating procedure is compatible with oxidized diamond surfaces thus well-suitable for diamond-based quantum technology. The results can directly impact applications of diamond materials in optically detected quantum sensing or fluorescence sensing in general. The polymer functionalization can also be used for any case where highly specific interaction with low fouling is desired.

1. Introduction

In the past two decades, synthetic diamond crystals have attracted rapidly increasing attention. Multiple disciplines including optics, electronics, quantum technology, analytical chemistry, and biology utilize specific and diverse properties of diamonds such as chemical inertness, biocompatibility, mechanical hardness, large electrochemical potential window, wide bandgap, broad optical transparency, and ability to accommodate numerous optically active point lattice defects.[1] Among the most used types of bulk, diamonds are chemical vapor deposited (CVD) and HPHT (high-pressure high temperature) diamonds. Vast and heterogeneous range of bulk diamond applications can be exemplified by boron-doped diamond electrodes in electroanalysis,[2] diamond coatings in implants[3,4] or dye-sensitized solar cells with diamond electrodes.[5,6]

An important and particularly interesting application area of a bulk diamond is quantum technology. Ultra-pure, single crystalline CVD and HPHT diamond crystals provide a nearly-ideal environment for hosting a negatively charged nitrogen–vacancy (NV^-) center,[7] a photoluminescent defect which can operate as a qubit with almost unlimited photostability. The electronic spin-dependent photoluminescence associated with NV^- centers enables both their optical readout and initialization to a known state. Development of physics related to NV^- centers led to advances in quantum technology and enabled seminal experiments such as demonstration of quantum computing[8] and quantum communication,[9] recording of NMR spectra in a nanometer-sized volume,[10] optical detection of the magnetic field in living cells,[11] and optoelectronic on-chip detection of magnetic resonance.[12]

R. Kumar, B. Yang, M. Hirtz
Institute of Nanotechnology (INT) & Karlsruhe Nano Micro Facility (KNMFi)
Karlsruhe Institute of Technology (KIT)
76344 Eggenstein-Leopoldshafen, Germany
E-mail: michael.hirtz@kit.edu

The ORCID identification number(s) for the author(s) of this article can be found under https://doi.org/10.1002/admi.202201453.

DOI: 10.1002/admi.202201453

J. Barton, M. Stejfova, P. Cigler
Institute of Organic Chemistry and Biochemistry
Czech Academy of Sciences
Flemingovo nam. 2, Prague 6, Prague 166 10, Czech Republic
E-mail: petr.cigler@uochb.cas.cz

A. Schäfer
nanoAnalytics GmbH
Heisenbergstraße 11, 48149 Münster, Germany

M. König
Institute of Functional Interfaces (IFG)
Karlsruhe Institute of Technology (KIT)
76344 Eggenstein-Leopoldshafen, Germany

P. Knittel
Fraunhofer IAF
Fraunhofer Institute for Applied Solid State Physics
Tullastrasse 72, 79108 Freiburg, Germany

Many of the above-mentioned applications require a chemical control of the surface termination which is useful for chemical normalization of the surface, attachments of appropriate functional moieties and creation of interfaces resistant to particular environments (biological, chemically aggressive etc.). In this view, several approaches to providing bulk diamond functionalization via sp^3-carbon chemistry have been developed and their successful applications have been demonstrated.[13]

For example, an elegant photochemical modification of hydrogenated diamond has been developed and investigated by Hamers and colleagues.[14] The terminal vinyl group of a bifunctional organic linker is connected to the diamond surface by a C–C bond via photografting initiated by 254 nm light.[15] The opposite end of the linker is then deprotected, releasing for example terminal amino group useful for the grafting of (bio)molecules. Various linkers and applications of this photografting technique have been demonstrated.[14,16,17] Another approach is based on the formation of C–C bonds upon the reaction of hydrogenated diamond with diazonium salts.[18] However, these and similar methods require a hydrogenated surface which contributes to charge switching of the spin-active NV^- center to the neutral NV^0 state which is undesirable for quantum sensing.[19,20]

In general, chemical modifications based on oxidized or fluorinated surfaces are the most suitable for quantum sensing.[21,22] Carboxylic groups present on the oxidized diamond surface are typically used for the attachment of biomolecules via amidic bonds.[23] Nevertheless, an "atomically" modified diamond surface (e.g., oxidized, hydrogenated) is well-known by its strong ability to adsorb biomolecules,[24] which is further dependent on the actual crystal orientation.[25] Protein fouling by nanodiamonds is very effective and can be utilized for protein extraction before mass spectroscopy analysis.[26] Oxidized diamond surfaces can be also modified using silanization followed by click chemistry,[27] however, such surface is quite hydrophobic and its protein-repelling properties have not been demonstrated. Diamond surface thus brings an additional challenge: for the construction of (bio)sensors selectively operating in biological fluids, a thin antifouling interface coating is required.

To prevent the non-specific interactions, coating of diamond surface with biomimetic self-assembled monolayers[28] or with covalently attached hydrophilic polymers[29] has been studied. In this case, nanodiamonds have been the main investigated type of diamond since their colloidal stabilization is critical for construction of fluorescence probes and nanosensors operating in a physiological environment.[30] On nanodiamonds, polymers serve not only as an antifouling interface, but also prevent particle aggregation and allow chemical conjugation of (bio)molecules[31–33] and/or sensing architectures.[34,35] Among the effectively sterically stabilizing electroneutral synthetic polymers are, for example, poly(glycerol)[36] and poly[*N*-(2-hydroxypropyl)methacrylamide, poly(HPMA).[37,38] Antifouling effect can be achieved also using modified serum albumins[39,40] and recombinant protein polymers.[41] Cationic polymers can provide additional electrosteric stabilization, however, the charged surface may then promote electrostatic adsorption of charged biomolecules[42] and modulate cell transfection.[43]

In contrast to nanodiamonds, the modification of bulk diamond with polymers is chemically more demanding because of lower reactivity, steric hindrance of the surface, and lower diffusion rate of the reactants. Nevertheless, the preparation of addressable microarrays on the 2D surface of bulk diamond crystals is an important aim since these platforms can be potentially used for high-throughput optical-based quantum biomolecular analysis using NV^- center. Although the construction of microarrays has been demonstrated on other carbon materials,[44] the current approaches enabling covalent attachment of biomolecules to bulk diamond are limited to the hydrogenated surface and have been developed for different types of analysis.[15,16,45]

Here we show a manufacturing technique providing printable and stable microarrays on oxidized diamond which is naturally compatible with quantum sensing. We utilize antifouling polymethacrylamide-based alkyne-bearing polymer based on *N*-(2-hydroxypropyl) methacrylamide (HPMA). The copolymer chains are covalently linked to the silanized diamond surface using "grafting through" radical polymerization and can be further used for click bioconjugations in an aqueous or physiological environment. To show the potential of this platform for construction of biosensors, we use microchannel cantilever spotting (μCS). We construct various microarrays, monitor attachment of model fluorescence dyes, investigate the interaction of the microarrays with proteins and demonstrate their chemo-selective and site-specific attachments. To facilitate the initial screening of manufacturing conditions we preoptimize the coating on glass substrates and transfer then the optimal types of coating to bulk diamond crystals.

2. Results and Discussions

2.1. Design and Preparation of the Substrates

The plasma-cleaned oxidized diamond or glass substrates were first modified in the liquid phase with 3-methacryloxypropyltrimethoxysilane (MMA-silane) which formed a methacrylate-terminated monolayer suitable for polymerization (**Figure 1**a). The copolymer was then immobilized using the "grafting through" method,[46] where a polymerizable methacrylate group is anchored onto the surface of a nanoparticle. The polymerization was started in the solution containing initiator (azobis(isobutyronitrile), AIBN, which avoids using toxic metal catalysts[47]) and monomers. In the course of the reaction, the preattached polymerizable moiety was integrated into the growing polymer chains.[48] Importantly, "grafting through" differs from the "grafting from" approach where functional initiators are chemically linked onto the nanoparticle surface to initiate the polymerization directly. The "grafting through" process is self-limiting and the amount of attached polymer is largely independent of the conditions under which the reaction is performed. Although the "grafting through" provides typically lower grafting densities and layer thicknesses than the "grafting from" approach, the polymerization is robust, error-tolerant, and easy to perform.[46]

Two different types of segments coexist in the scaffold of our copolymer, HPMA and *N*-propargyl methacrylamide (AlkMA). Poly(HPMA)[49] is a broadly used hydrophilic and biocompatible

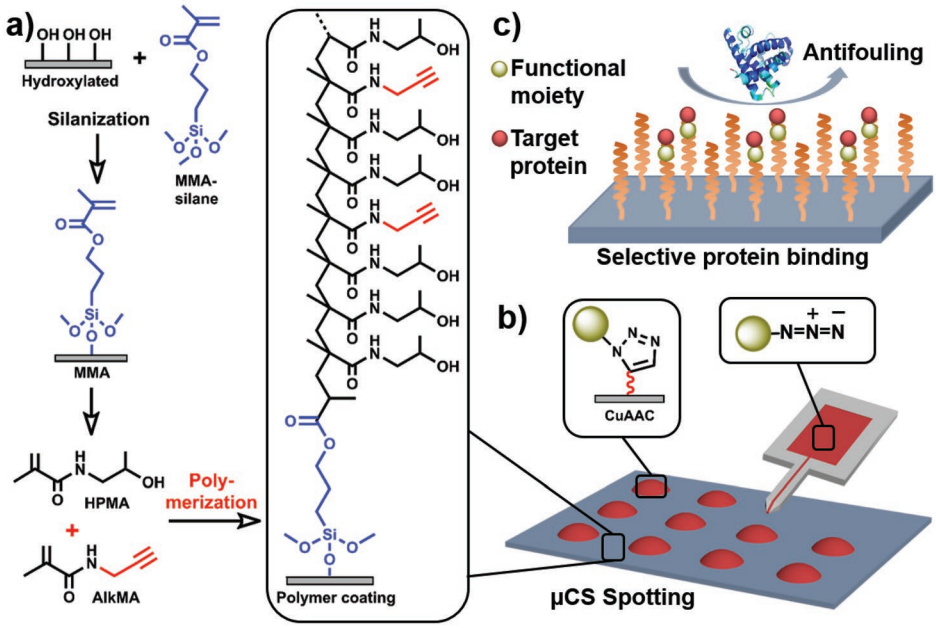

Figure 1. Schematic illustration of the chemical structure and µCS functionalization strategy of the poly(HPMA-*co*-AlkMA) polymer coatings. a) The fabrication route of the methacrylate-based, alkyne-bearing antifouling polymers. b) Creation of micropatterns by µCS on the reactive polymer surface. c) Selective binding of a target protein to the site-specifically functionalized polymer coating.

polymer, which provides exceptional antifouling properties.[50] Poly(HPMA) brushes have been successfully used for coating of gold surface plasmon resonance sensors.[51] A cross-linked poly(HPMA) photografted to various surfaces also provided strong surface hydrophilicity and excellent antifouling properties.[51,52]

Poly(HPMA) thus constitutes the main structure of our copolymer while the AlkMA segment was used to introduce alkyne groups to the copolymer structure. These alkyne groups are suitable for copper-catalyzed alkyne-azide cycloaddition (CuAAC) and are capable to attach different molecules or compounds to the coating surface.[47] Therefore, the poly(HPMA-*co*-AlkMA) remains protein-repellent without any additional background saturation and enables highly specific chemical functionalization by CuAAC click chemistry, which is fast, mild, and highly efficient.

Table 1. Summary of physical characterization (WCA, roughness, and thickness) of the film coatings. Every mean value with standard deviation was counted from 3 random measurements.

Items	WCA [°]	Roughness [nm]	Thickness [nm][a)]
Bare glass slide	45.2 ± 3.6	0.148 ± 0.026	–
Bare diamond surface	57.6 ± 2.3	0.187 ± 0.072	–
MMA-silanized on glass	66.3 ± 2.2	0.251 ± 0.031	1.6 ± 0.1
on diamond	65.6 ± 1.8	0.232 ± 0.066	–
Poly(HPMA-*co*-AlkMA) on glass	62.1 ± 3.9	1.682 ± 0.183	4.0 ± 0.1
on diamond	62.3 ± 3.1	1.033 ± 0.221	–

[a)]Films thickness was measured on silicon samples prepared in parallel with glass samples. The polymerization was implemented for one day.

2.2. Optimization of the Polymerization Procedure and Properties of Polymers

Both methacrylate-terminated glass and diamond substrates were modified with a mixture of HPMA and AlkMA providing a sufficiently dense layer of poly(HPMA-*co*-AlkMA). The resulting surfaces should exhibit excellent antifouling properties by the HPMA segments and contain alkyne groups that can bind azide derivatives by CuAAC reactions. For a basic check on the functionalization, each step was monitored by static water contact angle (WCA), atomic force microscopy (AFM), and ellipsometry. The results are summarized in **Table 1** and Figures S1 and S2 in Supporting Information.

WCA and surface roughness (root-mean-square roughness average, Ra) characterizations are the two common and facile approaches to monitor the process of surface modification because the surface tension and topography change when new substances are added to the material surface. As shown in Table 1, the WCA and roughness values of the bare glass surface are 45.2° and 0.148 nm, respectively, in agreement to prior results.[53] After silanization by methyl methacrylate on the glass surface, these values increase to 66.3° and 0.251 nm, respectively. In addition, the ellipsometric thickness of the MMA-silanized sample is 1.6 nm, which is also consistent with the self-assembled monolayer. After implementing polymerization, the roughness and thickness increased to 1.682 nm and 4.0 nm, respectively, while a slight decrease in WCA (62.1°) was observed. The same tendency of WCA and roughness change was found in diamond-based samples. The – for a hydrophilic backbone as HPMA – rather high WCA is probably caused by some wetting transparency to the underlying layer caused by the relative thin polymer film and by the alkyne

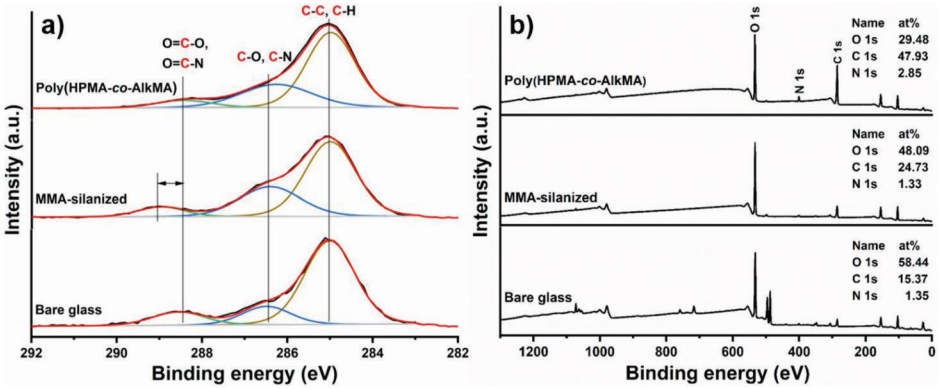

Figure 2. XPS characterization of different surfaces on glass substrates, a) at C 1s region, b) wide-scan spectra. The components resulting from corresponding chemical species are highlighted in red.

groups introduced, as was reported in similar systems addition after functionalization with small hydrophobic molecules.[54]

To further confirm the chemical functionalization steps, x-ray photoelectron spectroscopy (XPS) was performed on the samples. After MMA-silanization the sample surface shows three peaks at 285.0 eV, 286.4 eV, and 288.9 eV, which are derived from (C–C, C–H), (C–O), and (O–C=O), respectively (**Figure 2**). Comparing the XPS spectra in the C 1s region of the bare glass slide and MMA-silanized surface, the (C–O):(C–C, C–H) ratio increases from 0.21 to 0.45, which indicates a successful silanization process. XPS analysis of the C 1s region of poly(HPMA-*co*-AlkMA) shows signals assigned to (C–N) and (N–C=O) at 286.3 eV and 288.4 eV, respectively, derived from the amide component in the polymer skeleton.[55] As shown in Figure 2b, three main element signals are considered in the wide-scan spectrum of poly(HPMA-*co*-AlkMA), i.e., O 1s (530.7 eV), C 1s (288.7 eV), and N 1s (403.4 eV) in a 4:9:1 ratio. Considering the possibility of atmospheric contamination, this result is consistent with the elemental composition of the poly(HMPA) structure (2:7:1).[56] In addition, a single peak at 400.3 eV in the N 1s spectrum also confirms the amide nitrogen in the polymer chain (Figure S3 in Supporting Information).[55]

2.3. Evaluation of Antifouling Properties and Reactivity of the Polymer Coatings

In order to first verify the antifouling properties and the reactivity toward CuAAC reaction, polymer coatings on glass surfaces were used to print microarrays on them via µCS before demonstrating the functionalization with optimal preparation conditions on the diamond surfaces. During µCS, the tip of a microchannel carrying cantilever is repeatedly brought into contact with the substrate, allowing ink to flow from the ink reservoir on the chip connected to the microchannel to the substrate, generating micropatterns in a controlled environment. Each of the deposited droplets acts as a microreactor allowing the CuAAC reaction between azide moieties and alkyne terminals on the polymer substrate to take place.

To validate the CuAAC reaction on poly(HPMA-*co*-AlkMA) polymer-coated glass substrates and to characterize the resulting arrays, a fluorescent ink containing TAMRA-azide, Cu catalyst and sodium ascorbate was printed, followed by evaluation on a fluorescence microscope. **Figure 3** shows the images of TAMRA-azide functionalized micropatterns before

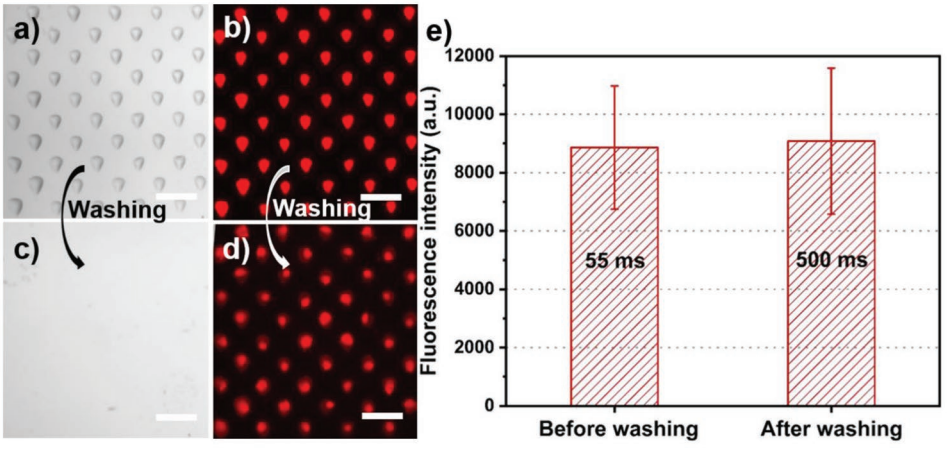

Figure 3. µCS printed TAMRA-azide dots on polymer-coated glass substrates. Pictures were captured in a) bright field and b) fluorescence (in Cy3 channel, exposure time 55 ms) before the washing step, and c) bright field and d) fluorescence (in Cy3 channel, exposure time 500 ms) after washing. e) Comparison of the fluorescence intensity before and after washing (data was collected on the image (b) and (d)). Scale bars are 50 µm.

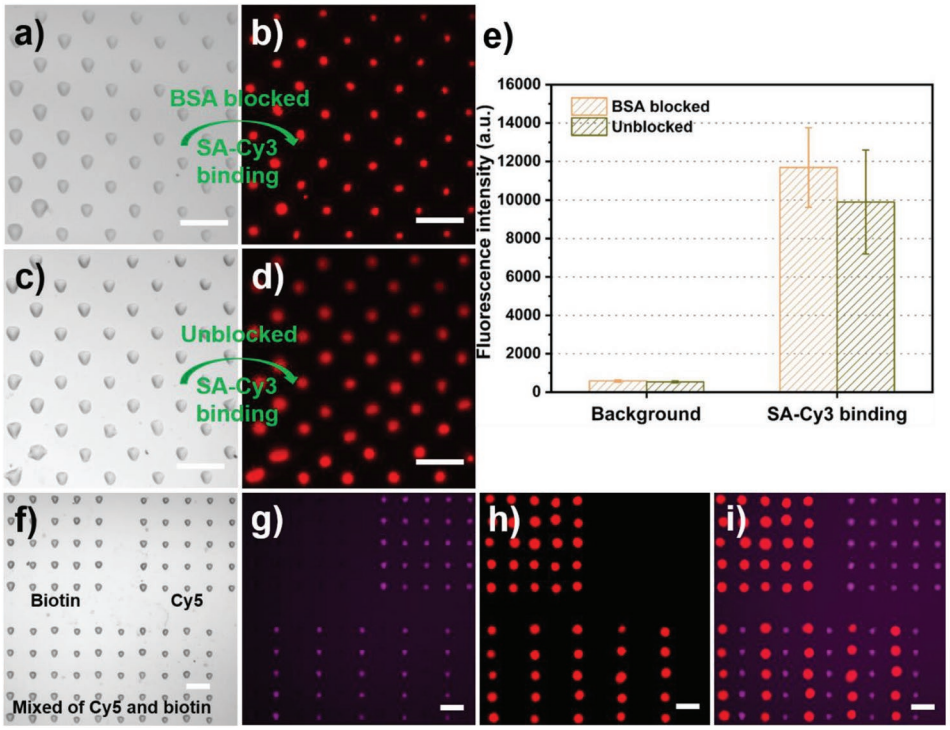

Figure 4. a) Biotin-azide printed dots and b) later incubated with SA-Cy3 after blocking with BSA-FITC. c) Biotin-azide printed dots and d) later incubated with SA-Cy3, but without any blocking step. e) Fluorescence intensity (in Cy3-channel) comparison between the samples blocked or unblocked with BSA-FITC. Exposure times for the fluorescence images are 100 ms. f) Optical image (before washing) of 5 × 5 matrices of biotin-azide (on the top left) and Cy5-azide (on the top right), and a multiplexed pattern (10 × 5) at the bottom part with alternating columns of biotin- and Cy5-azide. g) Cy5-channel (400 ms exposure) after washing, showing the Cy5 arrays and columns. h) The Cy3-channel (20 ms exposure) shows the biotin-azide columns after binding with SA-Cy3. i) Merged image by image (g) and (h). Scale bars are 50 µm.

(Figure 3a,b) and after (Figure 3c,d) washing with PBS solution and their fluorescence intensity comparison (Figure 3e). After washing, the pattern is still visible in the fluorescence channel, indicating that the azidated dye was firmly bound to the polymer surface. The fluorescence intensity can be deemed as a measure of the amount of bound azidated dye. Washing removed the excess ink and unbound azides, leaving behind only a covalently attached thin polymer layer bearing the TAMRA attached via triazole linkage. This is also reflected by a higher exposure time needed for the fluorescence imaging to reach the same intensity after washing (i.e., 55 ms before and 500 ms after washing). Considering the prolonged exposure time, around one-tenth of fluorescent molecules available in the ink was immobilized on the polymer coating. As a negative control experiment, a fluorophore (5-carboxyfluorescein-PEG3-BCN, FAM-BCN) not able to covalently bind to the alkyne in the polymer coating was spotted. After washing, no significant remaining fluorescence was observed (Figure S4, Supporting Information), further indicating that CuAAC taking place is needed to obtain stable attachment of fluorophores.

Next, protein binding trials with and without bovine serum albumin (BSA) blocking were implemented to assess the antifouling properties and targeting activity of the polymer coatings and microarrays. To do so, biotin-azide ink was used to create micropatterns on polymer-coated glass samples as described earlier. The high affinity of streptavidin toward biotin makes it an effective model to check the selective targeting and antifouling properties of the system by selective protein binding. Therefore, streptavidin-Cy3 (SA-Cy3) was employed as a fluorescent target protein in combination with or without a prior blocking step with FITC-conjugated BSA (BSA-FITC). To keep procedures as similar as possible, the samples which were not blocked by BSA were incubated with phosphate-buffered saline (PBS) as a mock process step. The typical outcomes are shown in **Figure 4**. First, as shown in Figure 4a,b, the polymer surface was blocked by BSA-FITC before implementing protein binding by SA-Cy3. In parallel, as shown in Figure 4c,d, another sample was directly incubated with SA-Cy3, without BSA blocking. As shown in Figure 4e, the fluorescence intensity (in Cy3- channel) on SA-Cy3 coupled arrays is almost the same regardless of BSA-blocking and both samples show only a very low background (measured in between the dot features). This means that the target protein – even without prior blocking – only binds to the biotinylated region and almost no protein fouling takes place at the unfunctionalized areas, showing excellent antifouling capabilities of the polymer coating. In addition, the use of BSA-FITC allows also for quantification of the BSA adsorbed during blocking (Figure S5 in Supporting Information).

In addition, to visualize BSA adhesion, the background signals (in FITC channel) reflecting adhered BSA and unspecific fluorescence of polymer itself on the samples (the same samples shown in Figure 4a-d) either blocked or unblocked by BSA-FITC were quantified as shown in Figure S5, Supporting Information. The low background signal seen in the unblocked

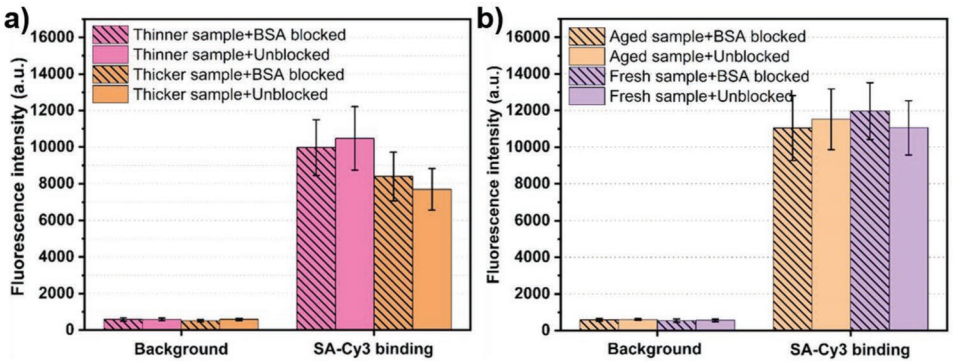

Figure 5. Fluorescence intensity (in Cy3 channel) of the samples incubated with SA-Cy3 with or without BSA blocking. Samples with a) different thicknesses and b) prepared at different ageing states of the underlying silane layer. The standard deviation was computed from 50 random spaces on an unfunctionalized area for background, and 50 SA-Cy3 bound spots for target protein binding.

sample is the auto-fluorescence of the polymer coating itself. On the BSA-FITC-blocked sample only a small increase in fluorescence is observed, reflecting the small amount of BSA that can attach to the polymer. Interestingly, the sites with biotin-azide functionalization bind even less BSA, letting them appear darker than the unfunctionalized surrounding polymer coating in contrast-enhanced images. This suppression of intensity is not seen on the non-blocked sample, indicating that it is not caused by an overall reduction in background fluorescence from the polymer coating itself, due to CuAAC. Together, these results further suggest the excellent antifouling properties and low background in fluorescence applications of the polymer coatings.

To demonstrate multiplexed patterns on the polymer coatings, azide inks either linked to a Cy5 fluorophore (Cy5-azide) or a biotin moiety (biotin-azide) were printed into arrays and alternating columns. Figure 4f-i shows optical micrographs of the multiplexed pattern after printing, washing and incubation of SA-Cy3. After completion of the CuAAC reaction between azide and alkyne moieties, with the excess ink solution washed off, only the Cy5-azide functionalized arrays and columns are visible in fluorescence (Figure 4g). Thereafter, SA-Cy3 was incubated on the sample to visualize the biotin functionalized columns (Figure 4h), making these features now appear in fluorescence, too. Figure 4i shows the merged fluorescence image of Cy5-azide and SA-Cy3 bound biotin-azide arrays.

Based on our knowledge, the preparation conditions and the composition of the polymer can have considerable influence on its antifouling properties and chemical reactivity.[57] In principle, the polymerization duration has a significant impact on coating thickness, and prolonged duration usually induces a thicker film coating. Therefore, to elucidate the coating thickness of polymer coating on its antifouling properties and reactivity, polymer-coated glass samples with two different thicknesses were prepared, polymerized for one day ("thinner", ellipsometric thickness was ≈4.0 nm), and polymerized for four days ("thicker", the ellipsometric thickness was ≈5.2 nm). After sample preparation, these samples were investigated with protein binding assays as described above and then evaluated using a fluorescence microscope. The corresponding fluorescence intensity (in Cy3 channel) for the different samples is shown in **Figure 5**a. The fluorescence intensity reveals that both types of samples give a similar low background value and thus a high signal-to-noise ratio, thus demonstrating excellent antifouling properties and chemical reactivity with azides. Moreover, the BSA blocking step again has no significant effects on antifouling properties as the same background and target signal values are shown. While error bars still overlap, the intensity of SA-Cy3 on the thicker sample is slightly lower than on the thinner sample. As the incubation protocols were kept same, this could mean that the thinner sample possesses a higher chemical efficiency, since the intensity can be deemed as the number of reactive alkyne sites on the polymer coating, that were translated into protein binding sites over the biotin-azide. In addition, since there was not much difference in thickness between "thinner" and "thicker" samples, the following experiments were carried out on the "thinner" samples, which also saved some time in substrate preparation.

As the silanized methacrylate monolayer is crucial in the polymer grafting procedure, also the effects of ageing of the silane layer on the antifouling properties and reactivity of the polymer was studied. For this purpose, polymers were attached to the silanized monolayers using the "grafted through" approach at two different ageing states, freshly prepared ("fresh") and aged for three months ("aged"). After that, a protein binding assay as described above was conducted and the samples were evaluated by fluorescence imaging. The related results are shown in Figure 5b. Both samples show almost the same intensity of background and bound protein after protein-binding. Consequently, the ageing state of the underlying silane layer has no significant influence on the antifouling properties and reactivity of the polymer coating.

2.4. Applying the Polymer Coatings to Diamond Surface

As a final step, the polymer coating prepared at optimal fabrication parameters was implemented on the diamond surface to endow it with protein repellency and clickable reactive sites. Our aim was suppressing unspecific background and raising thus the signal-to-noise ratio in array-based fluorescence imaging trials. Initially, a fluorescently labeled azide ink (Alexa488-azide) was patterned to the polymer-coated diamond surface. The azidated dye bound stably to the surface, with the

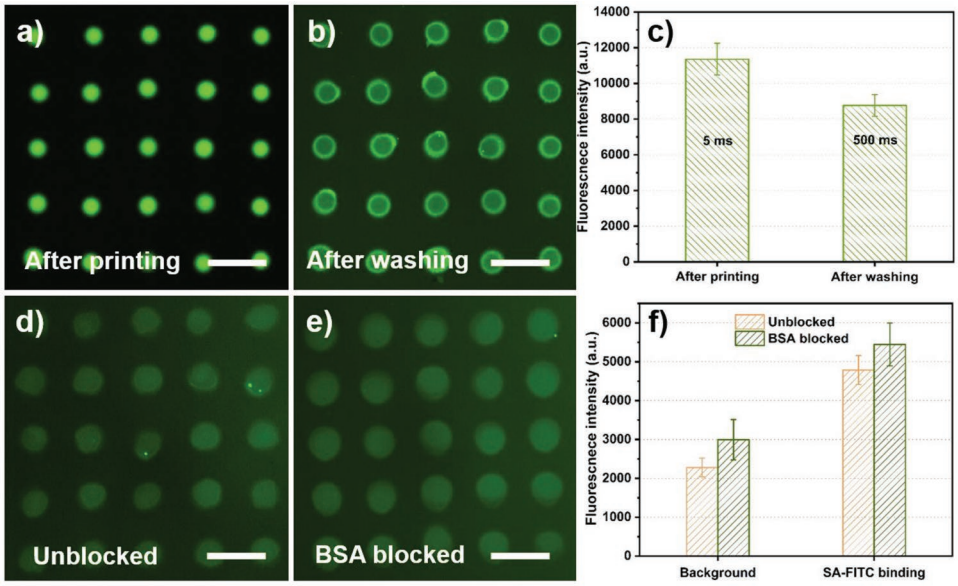

Figure 6. Fluorescence images of Alexa488-azide micropatterns on a polymer-coated diamond surface, a) after µCS printing (exposure time 5 ms), b) after washing (exposure time 500 ms). c) Fluorescence intensity collected from image (a) and (b). Fluorescence images of SA-FITC incubated biotin-azide micropatterns on polymer-coated diamond surfaces, d) direct incubation of SA-FITC, e) non-fluorescent BSA-blocking prior to SA-FITC incubation (exposure time 1 s for both (d) and (e)). f) Fluorescence intensity of background and spotted area collected from image (d) and (e). Scale bars are 50 µm in all images.

expected decrease in fluorescence intensity after washing off the excess ink (**Figure 6**a-c), as observed previously. Considering the prolonged exposure time after washing away the excess ink, around 1% of molecules available in the ink was immobilized to the diamond surface. Subsequently, protein binding trials were conducted on biotin-azide functionalized microarrays, similar to the above experiments. The diamond-based samples were subjected either to BSA blocking or remained unblocked before conducting protein binding. The results are shown in Figure 6d-f. The comparison of the fluorescence intensity (Figure 6f) shows that highly selective protein binding was achieved on the micropatterned polymer-coated diamond surface, with a high signal-to-noise ratio and low unspecific protein binding. This is in particular striking when comparing the fluorescence background on the polymer functionalized diamond with an unmodified control (Figure S6, Supporting Information). Interestingly, on the diamond surfaces BSA blocking even slightly increases the background intensity (through error bars still overlap).

3. Conclusion

In summary, a biocompatible methacrylate-based alkyne-bearing antifouling polymer coating [poly(HPMA-*co*-AlkMA)] for microarraying on glass and oxidized diamond substrates via µCS was presented in this work. The several nanometers thick polymer was grown using "grafting through" radical polymerization. The coating showed remarkable protein-repellent ability and was compatible with the site-specific functionalization via CuAAC click chemistry by µCS to enable covalently bound, arbitrarily designed or even multiplexed micropatterns. Our technique facilitates the introduction of selective protein binding sites on an otherwise highly protein-repellent polymer coating on the diamond and allows to omit additional passivation treatments while performing great in post-processing. Importantly, we designed the coating process to be compatible with an oxidized diamond surface which minimizes charge switching of the spin-active NV^- center to the neutral NV^0 state. Furthermore, the low thickness of the polymer layer is convenient for quantum sensing using NV centers in diamond. We believe that the presented surface architecture on diamond can facilitate the construction of microarray-based systems enabling detection using quantum technology, or, more generally, using fluorescence readout. In comparison to the current approaches, the µCS on diamond can significantly simplify the manufacturing of diamond-based chips, save analysis time and promote the prospects of the diamond in biosensing related applications.

4. Experimental Section

Materials and Chemicals: Toluene, chloroform, ethanol, and glycerol were purchased from Sigma-Aldrich (Germany). Tamra/Alexa488-azide and Cyanine 5 (Cy5)-azide were obtained from Thermo Fisher Scientific (Germany). Biotin-azide was obtained from Jena Bioscience (Germany). Streptavidin Cyanine-3 (SA-Cy3), 3-methacryloxypropyltrimethoxysilane (MMA-silane), copper sulfate ($CuSO_4{\cdot}5H_2O$), and sodium ascorbate (Na-As) were purchased from Sigma-Aldrich (Germany). Bovine serum albumin (BSA), bovine serum albumin-FITC (BSA-FITC), azobis(isobutyronitrile) (AIBN), and phosphate-buffered saline (PBS) were purchased from Sigma-Aldrich (Germany). Ultrapure water was produced in lab by an Arium Pro system from Sartorius (Germany). HPMA and AlkMA were synthesized and purified according to the previously published protocols,[58] what is important for obtaining high-quality homogeneous surfaces.

Diamond Films: Double-side polished (001) HPHT diamonds ($3 \times 3 \times 0.3$ mm^3, Element Six, UK) were used as a substrate and

overgrown with an ≈20 µm thick ultrapure CVD diamond film to suppress background fluorescence by the diamond substrate. An ellipsoidal microwave plasma chemical vapor deposition (MPCVD) (915 MHz) reactor with purified gases (hydrogen and methane) was employed for diamond growth.[59] After growth the samples were polished to achieve a surface roughness of below 1 nm. All samples were cleaned in a 3:1 mixture of sulfuric and nitric acid at 250 °C.

Substrates Preparation: Glass slides (10 × 10 mm, VWR, Germany) and diamond chips were cleaned by sonication in chloroform, ethanol, and water for 5 min each and then dried with nitrogen. Straight after, plasma treatment (10 sccm O_2, 0.2 mbar, and 100 W, ATTO plasma system, Diener electronics, Germany) was done 5 min for glass and 30 s for diamond, respectively. Subsequently, the hydroxylated substrates were immersed in a freshly prepared MMA-silane solution in toluene (1%, v/v) overnight at room temperature, and then the substrates were washed with toluene, ethanol, and water, and then dried under a nitrogen stream. The polymer was attached to the MMA-silanized surface by "grafted through" radical polymerization. Briefly, HPMA (700 mg, 4.82 mmol), AlkMA (35 mg, 0.06 mmol), and AIBN (200 mg, 1.22 mmol) were dissolved in DMSO (2.1 ml). After complete dissolving, the mixture was added to a flask containing silanized substrates. The polymerization was conducted under nitrogen at 55 °C for 1 day or for 4 days. While finishing, the substrates were washed with ethanol and water twice each and blown dry by nitrogen.

Ink Solutions Preparation: Ink solutions for CuAAC were based on copper sulfate (10 mM), and sodium ascorbate (20 mM) solutions in ultrapure water that were mixed with azidated compounds. An amount of 20% (v/v) of glycerol was added to the ink solutions as an ink carrier and to avoid too rapid evaporation of the ink solvent. The final concentration of the ink solution was 0.5 mg mL^{-1}.

Patterning via µCS: The patterns were created on an NLP 2000 instrument (Nanoink, USA), which was equipped with a microchannel cantilever (SPT-S-C30S, Bioforce, Nanosciences, USA). Before loading inks (0.2 µL), the tips were plasma cleaned by oxygen (0.2 mbar, 100 W, 20 sccm O_2, 2 min) to promote ink transfer, and then the inks were pushed into the microchannel by blowing with a nitrogen stream. All patterning processes (5 × 5 spot array with a pitch of 50 µm or 100 µm) were done at room temperature, with controlled humidity (30% RH) and dwell time (0.1 s). After printing, the samples were allowed to rest overnight at room temperature (RT) to complete the click reaction and then washed with water to remove the excess ink. To check the antifouling properties and the background signal of the polymer coating modified substrates by fluorescence imaging, the samples were printed with biotin inks and then covered with PBS and BSA (10 vol% in PBS) for 30 min individually, and then washed with PBS for protein (SA-Cy3) binding procedures (RT, 30 min). After that, the samples were washed three times with PBS and dried with nitrogen for microscope imaging.

Physico-Chemical Characterization: The static WCA was measured on an OCA-20 contact angle analyzer (DataPhysics Instruments GmbH, Germany) at room temperature. Concisely, a 3 µL water drop was dispensed on a sample surface, and the measurements were repeated three times for each sample to obtain the means and standard deviations. The film thickness was measured by spectroscopic ellipsometry (M 2000, Woollam Co., Inc., Lincoln NE, USA) on silicon substrates, which were prepared in parallel with a glass-based sample, in dry conditions at an incident angle of 65° in the wavelength range of λ = 370–900 nm. All measurements were evaluated with an optical box model on the software CompleteEase, and silicon substrates were all fitted with standard values for Si and SiO_2 as defined in the software. The thickness and the optical properties of the polymer layers were fitted with a Cauchy relation model. The roughness of the sample surface was evaluated by AFM (Dimension Icon, Bruker, Germany), at room temperature in the air in tapping mode (40 N m^{-1}, 325 kHz, HQ:NSC15/Al BS, MicroMasch, Germany). Three random positions were scanned for each sample (in 5 × 5 µm), and the original roughness Ra was extracted by the onboard software of the instrument. Apart from this, the analysis of chemical compositions of the surface in each step was identified by X-ray photoelectron spectroscopy (XPS) using a Thermo Scientific K-Alpha system (XPS, Thermo Fisher Scientific, East Grinstead, UK) with a base pressure of about 2×10^{-9} mbar. Excitation was done using monochromatic Al-Ka-X-rays. The energy calibration of the system was done according to ISO 15 472:2001 using copper, silver, and gold reference samples. The transmission function was determined using the build-in thermo standard method on a silver reference sample. Quantification of the measurement results was done using modified scofield sensitivity factors. A 400 µm X-ray spot was used for the analysis. On non-conducting samples, a flood gun was used for compensation of charging.

Optical Imaging: The optical images were captured on a Nikon Eclipse 80i upright fluorescence microscope (Nikon, Germany) equipped with an Intensilight illumination (Nikon, Germany), a Nikon DS Qi2 camera, and Cy5 and FITC and Tamra filters (Nikon Y-2E/C). The fluorescence intensities where extracted from the collected images by the built-in NIS-element software (Nikon, Germany).

Statistical Analysis: All data shown in this work were described as means ± standard deviations. The values of fluorescence intensity were obtained by an onboard software (NIS Elements AR 5.02.01, Nikon) of the microscope. The original data of WCA, thickness, and roughness were obtained by measuring 3 random points of each sample, and the means and standard deviations were computed on excel by the STDEVA formula.

Supporting Information

Supporting Information is available from the Wiley Online Library or from the author.

Acknowledgements

R.K. and B.Y. contributed equally to this work. The authors thank Lucie Drbohlavova for help with the development of the polymer coating and Vincent Mortet for stimulating discussions. This work was partly carried out with the support of the Karlsruhe Nano Micro Facility (KNMFi, www.knmf.kit.edu), a Helmholtz Research Infrastructure at Karlsruhe Institute of Technology (KIT, www.kit.edu). This work was supported by KNMF project Nr. 2020-023-028480. B. Y. acknowledges support by the China Scholarship Council fellowship (No. 201807040067, CSC, www.csc.edu.cn). P. C. acknowledges support by European Regional Development Fund, OP RDE, Project: CARAT (No. CZ.02.1.01/0.0/0.0/16_026/0008382). P. K. acknowledges financial support by the Fraunhofer Lighthouse Project Quantum Magnetometry (QMag).

Open Access funding enabled and organized by Projekt DEAL.

Conflict of Interest

The authors declare no conflict of interest.

Data Availability Statement

The data that support the findings of this study are available from the corresponding author upon reasonable request.

Keywords

antifouling polymer coating, copper catalyzed alkyne-azide cycloaddition, diamond surfaces, fluorescence imaging, microchannel cantilever spotting, selective protein binding

Received: July 1, 2022
Revised: August 15, 2022
Published online:

[1] Y. Yang, Q. Zhao, L. Liu, Y. Liu, C. Rosales-Guzmán, C.-W. Qiu, *Phys. Rev. Appl.* **2019**, *12*, 064007.
[2] S. Baluchova, A. Danhel, H. Dejmkova, V. Ostatna, M. Fojta, K. Schwarzova-Peckova, *Anal. Chim. Acta* **2019**, *1077*, 30.
[3] J. Liskova, O. Babchenko, M. Varga, A. Kromka, D. Hadraba, Z. Svindrych, Z. Burdikova, L. Bacakova, *Int. J. Nanomed.* **2015**, *10*, 869.
[4] M. Kalbacova, B. Rezek, V. Baresova, C. Wolf-Brandstetter, A. Kromka, *Acta Biomater.* **2009**, *5*, 3076.
[5] H. Krysova, L. Kavan, Z. V. Zivcova, W. S. Yeap, P. Verstappen, W. Maes, K. Haenen, F. Gao, C. E. Nebel, *RSC Adv.* **2015**, *5*, 81069.
[6] J. Bartoň, H. Krýsová, P. Janda, H. Tarábková, P. Ashcheulov, V. Mortet, A. Taylor, J. Vávra, P. Cígler, L. Kavan, *Appl. Mater. Today* **2018**, *12*, 153.
[7] C. E. Nebel, *Semicond.. Semimetals* **2020**, *103*, 73.
[8] L. C. M. V. Gurudev Dutt, L. Jiang, E. Togan, J. Maze, F. Jelezko, A. S. Zibrov, P. R. Hemmer, M. D. Lukin, *Science* **2007**, *316*, 1312.
[9] B. Hensen, H. Bernien, A. E. Dreau, A. Reiserer, N. Kalb, M. S. Blok, J. Ruitenberg, R. F. Vermeulen, R. N. Schouten, C. Abellan, W. Amaya, V. Pruneri, M. W. Mitchell, M. Markham, D. J. Twitchen, D. Elkouss, S. Wehner, T. H. Taminiau, R. Hanson, *Nature* **2015**, *526*, 682.
[10] F. S. T. Staudacher, S. Pezzagna, J. Meijer, J. Du, C. A. Meriles, F. Reinhard, J. Wrachtrup, *Science* **2013**, *339*, 561.
[11] D. Le Sage, K. Arai, D. R. Glenn, S. J. DeVience, L. M. Pham, L. Rahn-Lee, M. D. Lukin, A. Yacoby, A. Komeili, R. L. Walsworth, *Nature* **2013**, *496*, 486.
[12] M. N. P. Siyushev, E. Bourgeois, M. Gulka, J. Hruby, T. Yamamoto, M. Trupke, T. Teraji, J. Isoya, F. Jelezko, *Science* **2019**, *363*, 728.
[13] S. Szunerits, C. E. Nebel, R. J. Hamers, *MRS Bull.* **2014**, *39*, 517.
[14] E. C. L. Xiaoyu Wang, R. Franking, R. J. Hamers, *Acc. Chem. Res.* **2010**, *43*, 1205.
[15] W. Yang, O. Auciello, J. E. Butler, W. Cai, J. A. Carlisle, J. E. Gerbi, D. M. Gruen, T. Knickerbocker, T. L. Lasseter, J. N. Russell Jr., L. M. Smith, R. J. Hamers, *Nat. Mater.* **2002**, *1*, 253.
[16] T. L. C. C. Stavis, J. E. Butler, A. D. Radadia, R. Carr, H. Zeng, W. P. King, J. A. Carlisle, A. Aksimentiev, R. Bashir, R. J. Hamers, *Proc. Natl. Acad. Sci. USA* **2010**, *108*, 983.
[17] H. Krysova, J. Barton, V. Petrak, R. Jurok, M. Kuchar, P. Cigler, L. Kavan, *Phys. Chem. Chem. Phys.* **2016**, *18*, 16444.
[18] M. S. Simon, Q. Lud, R. Jordan, P. Bruno, D. M. Gruen, P. Feulner, J. A. Garrido, M. Stutzmann, *J. Am. Chem. Soc.* **2006**, *128*, 16884.
[19] V. Petráková, M. Nesládek, A. Taylor, F. Fendrych, P. Cígler, M. Ledvina, J. Vacík, J. Štursa, J. Kučka, *Phys. Status Solidi A* **2011**, *208*, 2051.
[20] M. V. Hauf, B. Grotz, B. Naydenov, M. Dankerl, S. Pezzagna, J. Meijer, F. Jelezko, J. Wrachtrup, M. Stutzmann, F. Reinhard, J. A. Garrido, *Phys. Rev. B* **2011**, *83*, 081304.
[21] S. Sangtawesin, B. L. Dwyer, S. Srinivasan, J. J. Allred, L. V. H. Rodgers, K. De Greve, A. Stacey, N. Dontschuk, K. M. O'Donnell, D. Hu, D. A. Evans, C. Jaye, D. A. Fischer, M. L. Markham, D. J. Twitchen, H. Park, M. D. Lukin, N. P. de Leon, *Phys. Rev. X* **2019**, *9*, 031052.
[22] J. Havlik, H. Raabova, M. Gulka, V. Petrakova, M. Krecmarova, V. Masek, P. Lousa, J. Stursa, H.-G. Boyen, M. Nesladek, P. Cigler, *Adv. Funct. Mater.* **2016**, *26*, 4134.
[23] H. S. Jung, K. C. Neuman, *Nanomaterials* **2021**, *11*, 153.
[24] M. Aramesh, O. Shimoni, K. Ostrikov, S. Prawer, J. Cervenka, *Nanoscale* **2015**, *7*, 5726.
[25] V. Damle, K. Wu, O. De Luca, N. Ortí-Casañ, N. Norouzi, A. Morita, J. de Vries, H. Kaper, I. S. Zuhorn, U. Eisel, D. E. P. Vanpoucke, P. Rudolf, R. Schirhagl, *Carbon* **2020**, *162*, 1.
[26] H. L. Khuong, C. H. Chen, J. L. Lin, T. N. Le, T. H. Pham, T. B. T. Le, X. C. Nguyen, V. C. Phan, H. H. Chu, W. W. Hsiao, T. M. P. Nguyen, D. M. Pham, *J. Proteome Res.* **2022**, *21*, 67.
[27] M. Davydova, A. de los Santos Pereira, M. Bruns, A. Kromka, E. Ukraintsev, M. Hirtz, C. Rodriguez-Emmenegger, *RSC Adv.* **2016**, *6*, 57820.
[28] J. Vavra, I. Rehor, T. Rendler, M. Jani, J. Bednar, M. M. Baksh, A. Zappe, J. Wrachtrup, P. Cigler, *Adv. Funct. Mater.* **2018**, *28*, 1803406.
[29] J. Neburkova, J. Vavra, P. Cigler, *Curr. Opin. Solid. State Mater Sci.* **2017**, *21*, 43.
[30] R. Li, T. Vedelaar, A. Mzyk, A. Morita, S. K. Padamati, R. Schirhagl, *ACS Sens.* **2022**, *7*, 123.
[31] F. J. Hsieh, S. Sotoma, H. H. Lin, C. Y. Cheng, T. Y. Yu, C. L. Hsieh, C. H. Lin, H. C. Chang, *ACS Appl. Mater. Interfaces* **2019**, *11*, 19774.
[32] J. Neburkova, F. Sedlak, J. Zackova Suchanova, L. Kostka, P. Sacha, V. Subr, T. Etrych, P. Simon, J. Barinkova, R. Krystufek, H. Spanielova, J. Forstova, J. Konvalinka, P. Cigler, *Mol. Pharmaceutics* **2018**, *15*, 2932.
[33] K. Kvakova, M. Ondra, J. Schimer, M. Petrik, Z. Novy, H. Raabova, M. Hajduch, P. Cigler, *Adv. Funct. Mater.* **2022**, *32*, 2109960.
[34] T. Rendler, J. Neburkova, O. Zemek, J. Kotek, A. Zappe, Z. Chu, P. Cigler, J. Wrachtrup, *Nat. Commun.* **2017**, *8*, 14701.
[35] J. Barton, M. Gulka, J. Tarabek, Y. Mindarava, Z. Wang, J. Schimer, H. Raabova, J. Bednar, M. B. Plenio, F. Jelezko, M. Nesladek, P. Cigler, *ACS Nano* **2020**, *14*, 12938.
[36] L. Zhao, T. Takimoto, M. Ito, N. Kitagawa, T. Kimura, N. Komatsu, *Angew. Chem.* **2011**, *50*, 1388.
[37] I. Rehor, H. Mackova, S. K. Filippov, J. Kucka, V. Proks, J. Slegerova, S. Turner, G. Van Tendeloo, M. Ledvina, M. Hruby, P. Cigler, *ChemPlusChem* **2014**, *79*, 21.
[38] P. Kovaricek, M. Cebecauer, J. Neburkova, J. Barton, M. Fridrichova, K. A. Drogowska, P. Cigler, J. M. Lehn, M. Kalbac, *ACS Nano* **2018**, *12*, 7141.
[39] B.-M. Chang, H.-H. Lin, L.-J. Su, W.-D. Lin, R.-J. Lin, Y.-K. Tzeng, R. T. Lee, Y. C. Lee, A. L. Yu, H.-C. Chang, *Adv. Funct. Mater.* **2013**, *23*, 5737.
[40] P. Moscariello, M. Raabe, W. Liu, S. Bernhardt, H. Qi, U. Kaiser, Y. Wu, T. Weil, H. J. Luhmann, J. Hedrich, *Small* **2019**, *15*, 1902992.
[41] T. Zheng, F. Perona Martinez, I. M. Storm, W. Rombouts, J. Sprakel, R. Schirhagl, R. de Vries, *Anal. Chem.* **2017**, *89*, 12812.
[42] V. Petrakova, V. Benson, M. Buncek, A. Fiserova, M. Ledvina, J. Stursa, P. Cigler, M. Nesladek, *Nanoscale* **2016**, *8*, 12002.
[43] S. Claveau, M. Kindermann, A. Papine, Z. V. Diaz-Riascos, X. Delen, P. Georges, R. Lopez-Alemany, O. M. Tirado, J. R. Bertrand, I. Abasolo, P. Cigler, F. Treussart, *Nanoscale* **2021**, *13*, 9280.
[44] L. M. S. M. R. Lockett, *Annu. Rev. Anal. Chem.* **2015**, *8*, 263.
[45] A. D. Radadia, C. J. Stavis, R. Carr, H. Zeng, W. P. King, J. A. Carlisle, A. Aksimentiev, R. J. Hamers, R. Bashir, *Adv. Funct. Mater.* **2011**, *21*, 1040.
[46] M. Henze, D. Mädge, O. Prucker, J. Rühe, *Macromolecules* **2014**, *47*, 2929.
[47] J. Slegerova, M. Hajek, I. Rehor, F. Sedlak, J. Stursa, M. Hruby, P. Cigler, *Nanoscale* **2015**, *7*, 415.
[48] L. Wu, U. Glebe, A. Böker, *Polym. Chem.* **2015**, *6*, 5143.
[49] J. Kopeče, H. Bažilová, *Eur. Polym. J.* **1973**, *9*, 7.
[50] A. R. Kuzmyn, L. W. Teunissen, P. Fritz, B. van Lagen, M. M. J. Smulders, H. Zuilhof, *Adv. Mater. Interfaces* **2022**, *9*, 2101784.
[51] L. Witzdam, Y. L. Meurer, M. Garay-Sarmiento, M. Vorobii, D. Soder, J. Quandt, T. Haraszti, C. Rodriguez-Emmenegger, *Macromol. Biosci.* **2022**, *22*, 2200025.
[52] C. Rodriguez-Emmenegger, E. Brynda, T. Riedel, M. Houska, V. Subr, A. B. Alles, E. Hasan, J. E. Gautrot, W. T. Huck, *Macromol. Rapid Commun.* **2011**, *32*, 952.
[53] S. M. M. Dadfar, S. Sekula-Neuner, U. Bog, V. Trouillet, M. Hirtz, *Small* **2018**, *14*, 1800131.

[54] Z. Fu, N. Zhang, J. Liu, T. Li, W. Xu, F. Wang, T. Wang, Z. Zhai, L. Liu, L. Mao, Y. Wu, *J. Colloid Interface Sci.* **2013**, *394*, 409.
[55] M. Vorobii, A. de los Santos Pereira, O. Pop-Georgievski, N. Y. Kostina, C. Rodriguez-Emmenegger, V. Percec, *Polym. Chem.* **2015**, *6*, 4210.
[56] E. Roeven, A. R. Kuzmyn, L. Scheres, J. Baggerman, M. M. J. Smulders, H. Zuilhof, *Langmuir* **2020**, *36*, 10187.
[57] A. de los Santos Pereira, T. Riedel, E. Brynda, C. Rodriguez-Emmenegger, *Sens. Actuators, B* **2014**, *202*, 1313.
[58] J. Neburkova, M. Hajek, I. Rehor, J. Schimer, F. Sedlak, J. Stursa, M. Hruby, P. Cigler, in *Integrin Targeting Systems for Tumor Diagnosis and Therapy* (Ed: E. Patsenker), Springer, New York **2018**, p. 169.
[59] C. W. M. Füner, P. Koidl, *Appl. Phys. Lett.* **1998**, *72*, 1149.